SCIENTIFIC REPORTS

OPEN

SUBJECT AREAS:
PHYSICS
MATERIALS SCIENCE

Received
20 February 2014

Accepted
14 April 2014

Published
9 May 2014

Correspondence and requests for materials should be addressed to A.C. (Alex.Chroneos@open.ac.uk) or U.S. (Udo.Schwingenschlogl@kaust.edu.sa)

Carbon related defects in irradiated silicon revisited

H. Wang[1], A. Chroneos[2,3], C. A. Londos[4], E. N. Sgourou[4] & U. Schwingenschlögl[1]

[1]PSE Division, KAUST, Thuwal 23955-6900, Saudi Arabia, [2]Engineering and Innovation, The Open University, Milton Keynes MK7 6AA, United Kingdom, [3]Department of Materials, Imperial College, London SW7 2AZ, United Kingdom, [4]University of Athens, Solid State Physics Section, Panepistimiopolis Zografos, Athens 157 84, Greece.

Electronic structure calculations employing hybrid functionals are used to gain insight into the interaction of carbon (C) atoms, oxygen (O) interstitials, and self-interstitials in silicon (Si). We calculate the formation energies of the C related defects $C_i(Si_I)$, C_iO_i, C_iC_s, and $C_iO_i(Si_I)$ with respect to the Fermi energy for all possible charge states. The $C_i(Si_I)^{2+}$ state dominates in almost the whole Fermi energy range. The unpaired electron in the $C_iO_i^+$ state is mainly localized on the C interstitial so that spin polarization is able to lower the total energy. The three known atomic configurations of the C_iC_s pair are reproduced and it is demonstrated that hybrid functionals yield an improved energetic order for both the A and B-types as compared to previous theoretical studies. Different structures of the $C_iO_i(Si_I)$ cluster result for positive charge states in dramatically distinct electronic states around the Fermi energy and formation energies.

Silicon (Si) is the basic material for numerous microelectronic, photovoltaic and sensor devices. Its electronic properties are known to be significantly affected by the presence of impurities and defects, which play an increasingly important role with the miniaturization of devices. Carbon (C), along with oxygen (O), is the most common and important impurity in Si. C is being incorporated in the Si lattice inadvertently during the growth. It mainly originates[1–5] from the poly-crystalline starting material, from graphitic components in the equipment or/and from gaseous contaminants developed during the growth process. C is isovalent with Si and occupies substitutional sites (C_s), which are electrically neutral. Nevertheless, the introduction of C in the lattice leads to local strain, due to its smaller size as compared to Si. Its presence is evidenced in infrared spectra by a localized vibrational mode at 607 cm^{-1}. Conversely, O impurities (which are likewise electrically neutral) occupy interstitial sites (O_i) within the Si lattice. Their presence is evidenced in infrared spectra by a number of localized vibrational modes, the most important among them at 1106 cm^{-1}. Both impurities are highly electronegative and chemically very reactive. They readily form bonds with Si atoms, with other defects and impurities, and between them. For instance in as-grown Cz-Si, modes at 589 cm^{-1}, 640 cm^{-1}, and 690 cm^{-1} have been correlated[4] with C-O complexes, in particular C_s-O_i pairs.

Upon irradiation, for instance with electrons of 1–2 MeV energy, vacancies and Si interstitial (Si_I) atoms are initially formed. Importantly, in spite of various suggestions[6] in the past, there is no adequate experimental evidence for any interaction between vacancies and C atoms. However, it is established[7,8] that most of the Si_I are readily trapped by C_s, which are pushed to interstitial sites according to the Watkins displacement reaction $C_s + Si_I \rightarrow C_i$. Two localized vibrational modes at 922 and 932 cm^{-1} have been correlated[9] with this defect in low temperature irradiated Si. C_i also introduces in-gap states[10]. The defect is unstable at room temperature and upon migration interacts promptly with O_i and C_s to form C_iO_i and C_iC_s pairs. At least six localized vibrational modes have been correlated with the C_iO_i defect. The best known appears at 865 cm^{-1} and, as the strongest, is used for calculating the defect concentration[11] by a calibration coefficient of $1.1 \cdot 10^{17}$ cm^{-2}. The C_iC_s defect is bistable and at least eleven localized vibrational modes are correlated with it in both configurations. All of them can be detected by low temperature measurements[12] and the one at 544 cm^{-1} even can be seen[13] at room temperatures. For the calculation of the defect concentration a calibration coefficient of 1.5×10^{15} cm^{-2} is used[11] Notably, a third configuration, the <100> C-C dumbbell, was proposed by Liu *et al.*[14] combining theoretical and experimental work. It was calculated that this configuration energetically is lower than the two bistable structures. Importantly, both the C_iO_i and C_iC_s defects introduce[4,15] states within the Si band gap, affecting the efficiency of the corresponding devices. Thus, numerous experimental and theoretical studies have been performed[16–20] to investigate the structure, properties, and behavior.

C-related defects are technologically paticularly important. For example the C_iC_s defect is utilized to improve the performance of Si optical emitters[21–24]. Additionally, the C_i, C_iO_i, and C_iC_s defects usually act in the course of

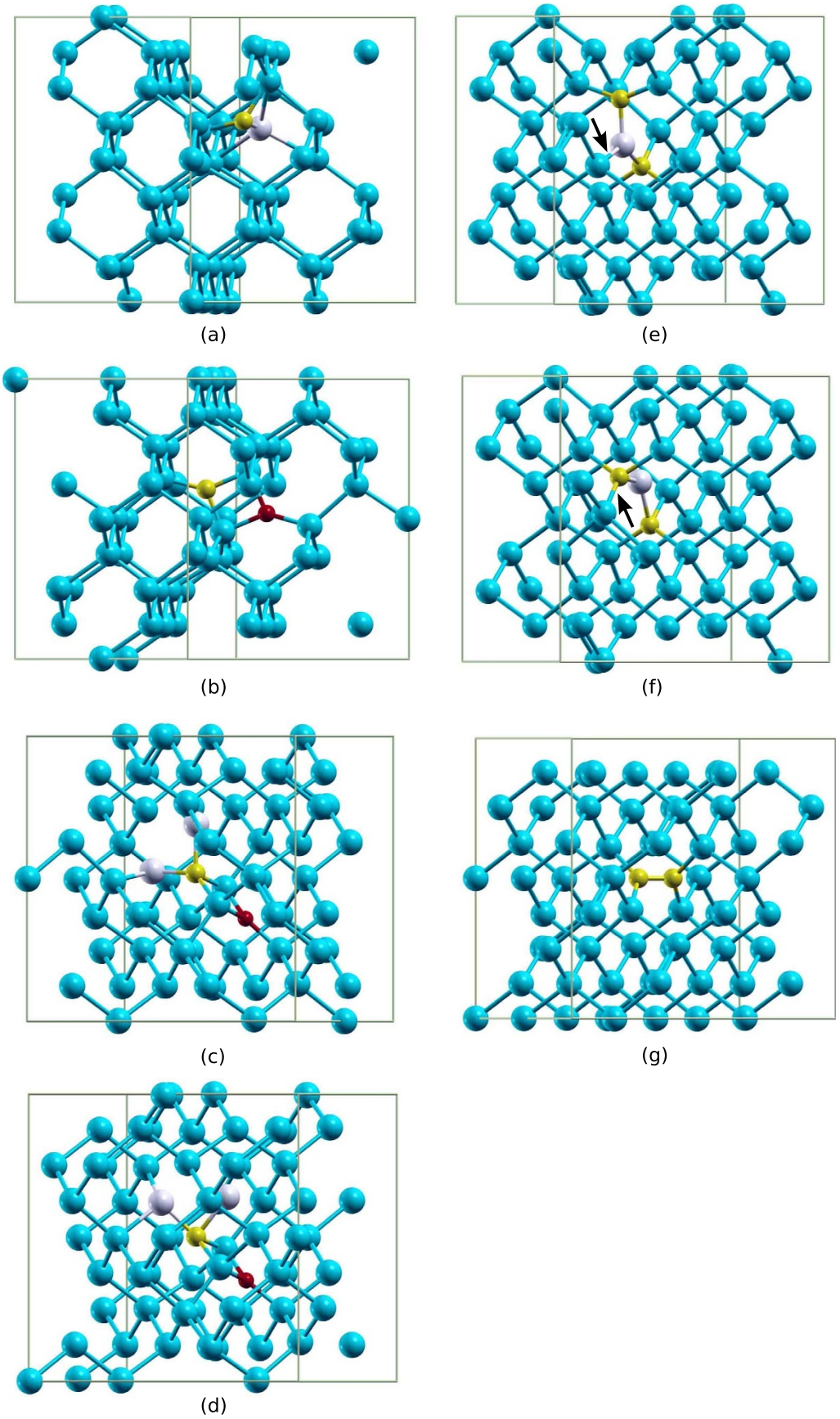

Figure 1 | Structures of (a) C_i (Si_I), (b) C_iO_i, (c) $C_iO_i(Si_I)_a$, (d) $C_iO_i(Si_I)_b$, (e) A-type C_iC_s, (f) B-type C_iC_s, and (g) C-type C_iC_s. Big blue spheres are Si atoms, medium yellow spheres C atoms, and small red spheres O atoms. The Si_I atom in C_i (Si_I), the Si atom connecting two C atoms in A-C_iC_s and B-C_iC_s, and the two Si atoms that show a significant position change between the two $C_iO_i(Si_I)$ structures are marked in gray. The breaking and forming bonds during the transition between A-C_iC_s and B-C_iC_s are highlighted by arrows.

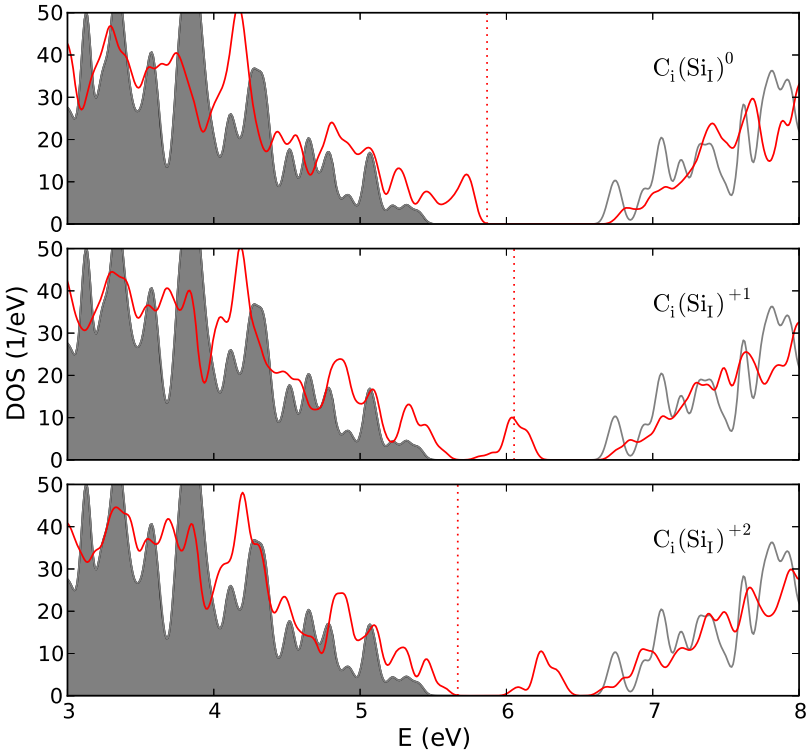

Figure 2 | Total DOSs of pristine Si (gray) and the $C_i(Si_I)$ defect (red). The states left of the dotted line are occupied.

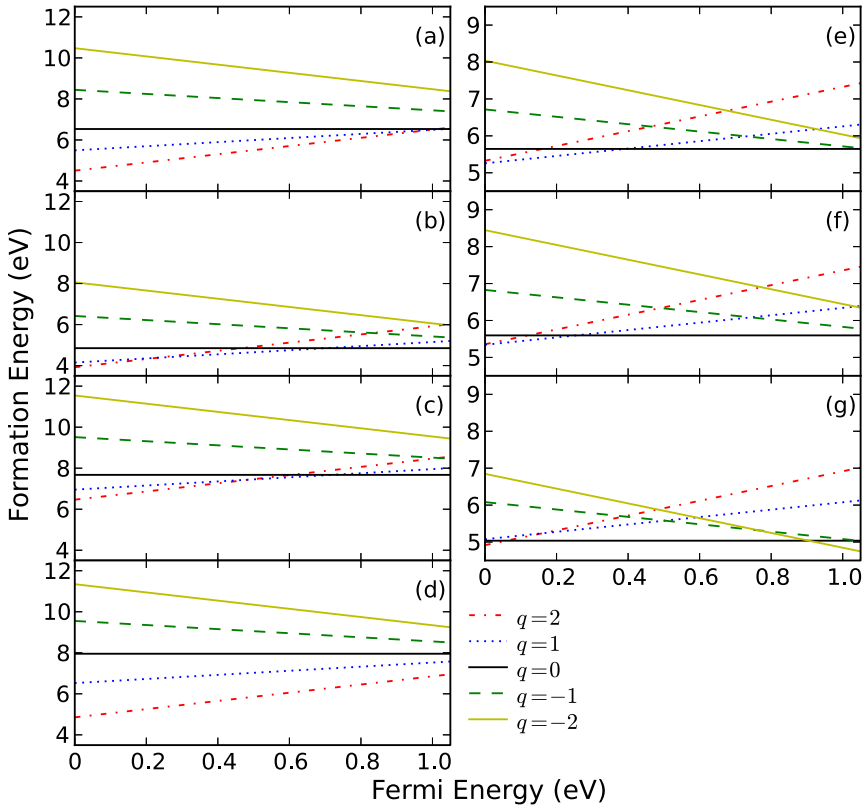

Figure 3 | Formation energies of the (a) C_i (Si_I), (b) C_iO_i, (c) $C_iO_i(Si_I)_a$, (d) $C_iO_i(Si_I)_b$, (e) A-type C_iC_s, (f) B-type C_iC_s, and (g) C-type C_iC_s defects with respect to the Fermi energy.

Table I | Transition levels (eV) between charge states for the $C_i(Si_I)$, C_iO_i, C_iC_s, and $C_iO_i(Si_I)_\alpha$ defects

Transition level	$C_i(Si_I)$	C_iO_i	A-C_iC_s	B-C_iC_s	C-C_iC_s	$C_iO_i(Si_I)_\alpha$
(++/+)	0.99	0.23	---	---	0.16	0.49
(++/0)	1.01	0.46	0.16	0.12	0.06	0.60
(+/0)	1.04	0.70	0.39	0.25	---	0.72
(0/−)	---	---	---	---	1.05	---
(0/—)	---	---	---	---	0.91	---
(+/−)	---	---	0.73	0.74	0.50	---
(+/—)	---	---	0.93	1.03	0.59	---
(++/−)	---	0.83	0.46	0.49	0.39	1.02
(−/—)	---	---	---	---	0.76	---
(++/—)	---	1.03	0.68	0.77	0.48	---

irradiation as nucleation centers for self-interstitials and complexes such as $C_i(Si_I)$, $C_iO_i(Si_I)$ and $C_iC_s(Si_I)$[25–28]. Notably, it was previously concluded, based on numerical simulations, that the capture radius of self-interstitials at C_iO_i is more than 3 times larger than at C_s[4]. Given the significance of self-interstitials for the Si properties, any contribution towards the understanding of their defect processes is crucial. For example, $C_i(Si_I)$ that has a significant role in the C aggregation processes in Si can impact the transient enhanced diffusion of boron[27]. Two infrared bands at 953 cm^{-1} and 966 cm^{-1} have been attributed to the $C_i(Si_I)$ complex, while those at 940 cm^{-1} and 1024 cm^{-1} belong to the $C_iO_i(Si_I)$ complex.

In the present study, we use hybrid density functional theory to characterize the critical C-related defects. In particular, we investigate the binding energies of the basic $C_i(Si_I)$, C_iO_i, C_iC_s, and $C_iO_i(Si_I)$ defects as well as the formation energies with respect to the Fermi energy for all possible charge states.

Results and discussion

Isolated defects. Before considering both defect pairs and clusters we investigated their constituent components C_s, C_i, O_i, and Si_I. We reproduce the structure of O_i according to Ref. 29 and the references therein. The O interstitial is bonded to two Si atoms forming a non-linear Si-O-Si pseudo-molecule. The two Si-O bond lengths are 1.63 Å and 1.64 Å, and the Si-O-Si bond angle is 151°. The charge neutral states of C_s and O_i dominate in the whole Fermi energy range, where the formation energies are 2.22 eV and 1.95 eV, respectively. These values are in good agreement with the heat of solution of substitutional C (2.30 eV) and interstitial O (1.65 ± 0.15 eV) in Cz-Si, as determined by Bean and Newman[30]. The <1 0 0> dumbbell C_i structure is also implemented in present study. It is the most favorable configuration according to Zirkelbach *et al*[31]. The dumbbell of C and Si atoms occupies a Si site with a bond distance of 1.75 Å. In the +1 charge state the unpaired electron is mainly located on the C interstitial, whereas in the −1 charge state the Si atom in the dumbbell traps the wave function of the electron more than other Si atoms because it loses valence charge to the C atom due to the higher electronegativity. Spin polarized HSE calculations show a lowering of the total energy for the charge +1 state by 0.27 eV as compared to spin degenerated calculations. C_i favors the +2 charge state at low Fermi energy (the formation energy is 3.42 eV for a Fermi energy of 0 eV), the +1 charge state in the middle of the band gap, and the 0 charge state with a formation energy of 4.50 eV in the high Fermi energy range. This value is larger than the 3.72 eV calculated within the general gradient approximation[31]. The charge transition levels amount to 0.23 eV (++/+) and 0.85 eV (+/0).

Si self-interstitials at hexagonal and tetrahedral sites[32] are studied, finding for the formation energy 4.36 eV and 4.72 eV, respectively. These values are larger than those obtained by previous theoretical work[33] employing the local density approximation (3.31 eV and 3.43 eV) and the generalized gradient approximation (3.80 eV and 4.07 eV), whereas the diffusion quantum Monte Carlo method results in 4.70 eV and 5.50 eV. Our calculations are consistent with the experimental value of 4.85 eV reported in Ref. 34.

Defect pairs. The most stable configuration of the $C_i(Si_I)$ defect is presented in Fig. 1(a). The Si-C dumbbell partially shares the

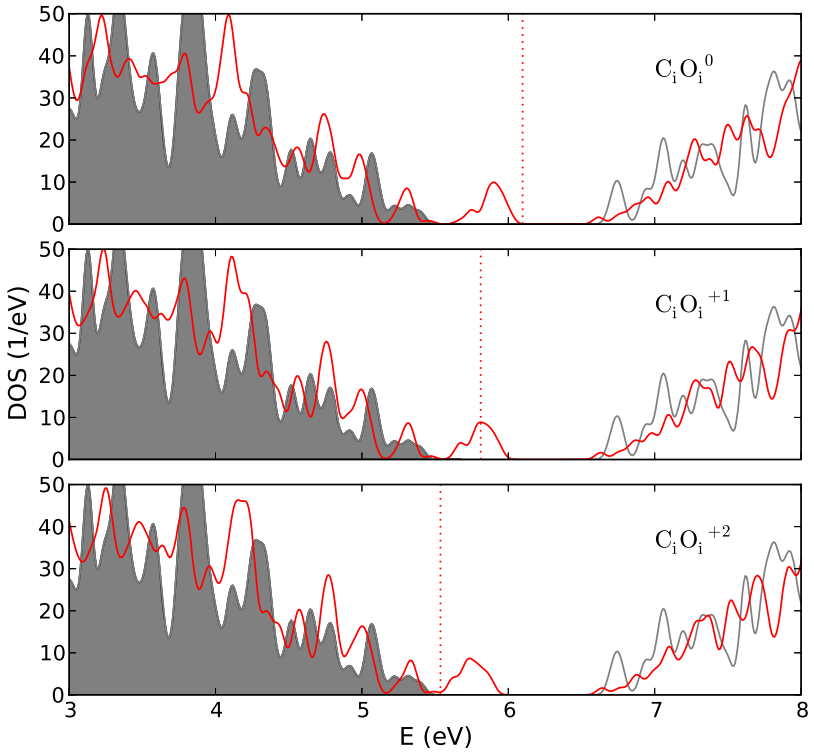

Figure 4 | Total DOSs of pristine Si (gray) and the C_iO_i defect (red). The states left of the dotted line are occupied.

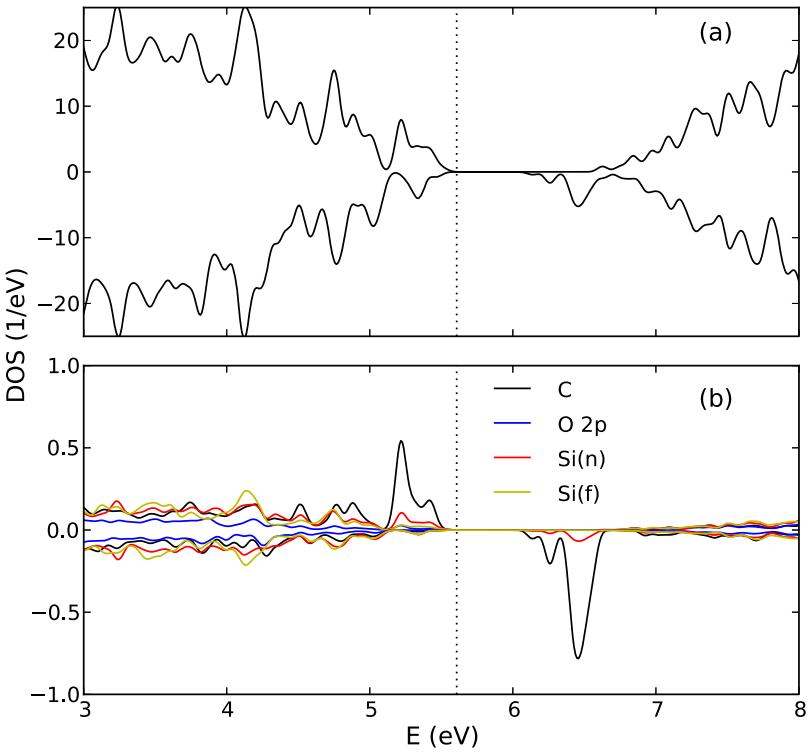

Figure 5 | Spin polarized (a) total and (b) partial DOSs of the C_iO_i defect. Si(n) and Si(f) denote the Si atoms nearest to and farthest away from the defect pair, respectively. The states left of the dotted line are occupied.

interstitial site and the Si atoms surrounding the defect pair are slightly shifted off their original positions. The C atom is threefold coordinated. Total densities of states (DOSs) in Fig. 2 show that the defect states gradually become separated from the valence band as the system receives more and more positive charge. We note that the band gap of pristine Si is calculated to be 1.05 eV using HSE, which resembles the experimental value of 1.17 eV[35]. The differences in the electronic structures arise from the distortion of the C-Si dumbbell and its neighboring atoms. The C-Si bond distances are reduced from 1.80 Å, 1.82 Å, and 1.82 Å in the charge neutral state to 1.77 Å, 1.79 Å, and 1.80 Å, respectively, in both positively charged states (which have the same C-Si bond distances). In addition, the orientation of the C-Si dumbbell is changed. The angle between the dumbbell and the [101] direction is 16°, 24°, and 29° for the 0, +1, and +2 charge state, respectively. The formation energies for the $C_i(Si_I)$ defect, see Fig. 3(a), indicate that the +2 state is more favorable than other charge states up to high Fermi energy. The transition levels between charge states are given in Table I.

The structure of the C_iO_i defect obtained in this work is consistent with the results of previous studies[17,18]. The C and O interstitials form with Si a ring, see Fig. 1(b), where the three O-Si bond lengths amount to 1.75 Å, 1.78 Å, and 1.86 Å, and the three C-Si bond lengths to 1.77 Å, 1.78 Å, and 1.79 Å. The Si-O-Si and Si-C-Si angles are 89° and 92°, respectively. Total DOSs for this system are shown in Fig. 4. The electronic structure of the $C_iO_i^0$ defect indicates that the valence bands and conduction bands occupy almost the same energy range as for pristine Si except for the fact that the defect states, which contain two electrons, shift up into the band gap. The center of the defect states is found about 0.35 eV above the valence band, which agrees well with the value of 0.38 eV as reported experimentally in Ref. 36.

Due to a pronounced DOS peak at the Fermi energy in the case of the $C_iO_i^+$ defect, HSE calculations with spin polarization are employed. We find a lowering of the total energy by 0.25 eV and a magnetic moment of 0.29 μ_B on C. Magnetic moments on other atoms are negligible. This result agrees with the electron paramagnetic resonance study of the $C_iO_i^{+1}$ defect in Ref. 16, which has found that the unpaired electron resides mainly on the C atom. Spin polarized total and partial DOSs for the $C_iO_i^+$ defect are plotted in Fig. 5. The Si atoms nearest to and farthest away from the defects are addressed as examples. For C and Si we show the sum of the s and p states because of the s-p hybridization. We find that the defect states are mainly due to the C interstitial, whereas the Si atoms around the defect give minor contributions. Hence, the C interstitial has a much larger magnetic moment than any other atom. As to be expected, Si atoms close to the C_iO_i pair contribute more to the defect states than Si atoms with larger distance. The formation energy of the defect C_iO_i as a function of the Fermi energy for different charge states is shown in Fig. 3(b), where the energy of the spin polarized calculation is used for $C_iO_i^+$. Due to the energy gain by spin polarization, we find that the stable state transits from +2 to +1 and then to 0 charge as the Fermi energy increases.

Figures 1(e), (f), and (g) present the three stable configurations of the C_iC_s defect. The A- and B-types[37] are established since long, whereas the C-type more recently has been demonstrated by first principles calculations to be the most stable configuration[31]. The bond lengths around the defects obtained in the present study, compare Table II, are consistent with the results in the literature[19,20,31]. The fourfold coordinated substitutional C atom in A-C_iC_s is denoted as C_s, the threefold coordinated C interstitial occupying a regular lattice site together with a Si as C_i, and the Si atom bonding with two

Table II | Bond distances (Å) around the A-, B-, and C-C_iC_s defects

A-C_iC_s	C_s-Si	C_i-Si	Si_{2C}-C
	1.88, 1.99, 1.99, 2.03	1.75, 1.83, 1.83	1.75, 1.88
B-C_iC_s	C_s-Si	C_i-Si	Si_{2C}-C
	1.85, 1.94, 2.01, 2.01	1.88, 1.96, 1.96, 2.04	1.85, 1.88
C-C_iC_s	C-Si	C-C	
	1.89	1.42	

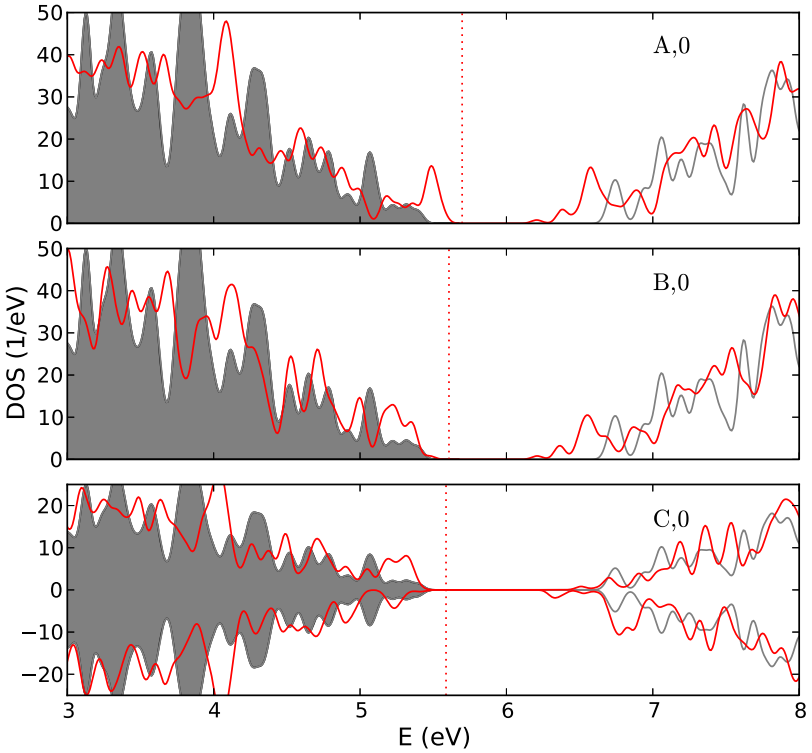

Figure 6 | Total DOSs of pristine Si (gray) and the A-, B-, and C-type C_iC_s defects (red) in the 0 charge state. The states left of the dotted line are occupied.

C atoms as Si_{2C}. Compared with A-C_iC_s, the Si_{2C}-Si bond breaks and a C_i-Si bond forms in B-C_iC_s. Although the C interstitial is now fourfold coordinated and substitutes the position of Si, we keep the notation as C_i for systematic reasons. In C-C_iC_s, the C-C pair along the <100> direction occupies a regular Si lattice site. Its bond length (1.42 Å) is shorter than in diamond or graphite. The fact that the four C-Si bonds (1.89 Å) are longer than the C-C bond implies that the C-Si interaction is weaker than the C-C dumbbell interaction.

The total DOSs for the 0 charge A-, B- and C-C_iC_s defects are depicted in Fig. 6. In A-C_iC_s the C_i has one dangling electron, leading to a peak below the Fermi energy. The 6.5 eV peak is mainly due to the localized unoccupied Si_{2C} states, which are caused by the two C nearest neighbors with higher electronegativity. Exactly the same situation is encountered in B-C_iC_s. A large portion of the electron trapped by the C_iC_s defect thus resides on Si_{2C}. Since C_i is fourfold coordinated in B-C_iC_s, the Si_{2C} atom keeps more valence charge, see the pronounced DOS at 5.2 eV. Also, both C atoms are in fourfold coordination and therefore give no significant contribution to this peak. The fact that each C atom in C-C_iC_s has a dangling electron is demonstrated by localized states at the Fermi energy in the spin degenerate DOS (not shown). The spin polarized DOS in Fig. 6 shows a clear spin splitting that results in magnetic moments on the C atoms. In the +1 and −1 states the wave function of the removed/trapped electron is shared by both C atoms.

Table III | Total energy differences (eV) for the ground states of the A- and B-C_iC_s defects for different charges. The numbers in brackets refer to spin polarized calculations

	A^+-B^+	A^0-B^0	A^--B^-
Experiment[a]	−0.02	0.02	−0.04
MINDO/3-Si_{38}[b]	−0.62	0.34	---
MINDO/3-Si_{41}[b]	−0.38	0.51	---
Cluster[c]	−0.43	−0.35	−0.50
Local density approximation[d]	---	0.11	---
This work PBEsol	0.15 (0.14)	0.20	0.23 (0.23)
This work HSE	−0.09 (−0.29)	0.04	0.07 (0.14)

[a]Reference 37.
[b]Reference 38.
[c]Reference 19.
[d]Reference 20.

The experimental energy differences[37] between A- and B-C_iC_s indicate that the A-type is more stable in the +1 and −1 charge states, whereas the B-type is more stable in the 0 charge state. For comparison, the results obtained by this and by previous studies are summarized in Table III. Those calculated by the PBEsol functional for the 0 charge state agree with the experiment only in the energetic order while the value is much larger. The HSE functional, on the other hand, yields results that agree with the experiment[37] much better than previous theoretical findings[19,20,38], except for the −1 charge state where the deviation from the experimental value is 0.11 eV. This discrepancy between the theoretical and experimental energy differences may be due to the fact that for A- and B-$C_iC_s^{-1}$ the wave function of the unpaired electron is delocalized, as demonstrated by experiments[37], while such a scenario is not well described by the HSE functional. Spin polarized calculations are performed with both the PBEsol and HSE functionals. PBEsol gives almost the same total energies as the spin degenerate calculations, while HSE lowers the total energies of A-type $C_iC_s^{+1}$ and B-type $C_iC_s^{+1}$ and $C_iC_s^{-1}$ by significant amounts of 0.22 eV, 0.02 eV, and 0.07 eV, respectively. Therefore, the energy difference between the two types is now −0.29 eV for the +1 charge state and 0.14 eV for the −1 charge state. In the case of A-$C_iC_s^{+1}$ the spin polarization delocalizes the occupied C_i DOS and shifts the unoccupied C_i DOS to higher energy. For B-type $C_iC_s^{+1}$ and $C_iC_s^{-1}$, respectively, the removed and trapped electron resides mainly on Si_{2C}. The energy of the charge neutral C-type C_iC_s defect is 0.11 eV higher than that of the A-type defect in the spin degenerate calculation, but 0.61 eV lower when spin polarization is taken into account. In addition, spin polarization lowers the energies of the +1 and −1 charge states by 0.20 eV and 0.23 eV, respectively.

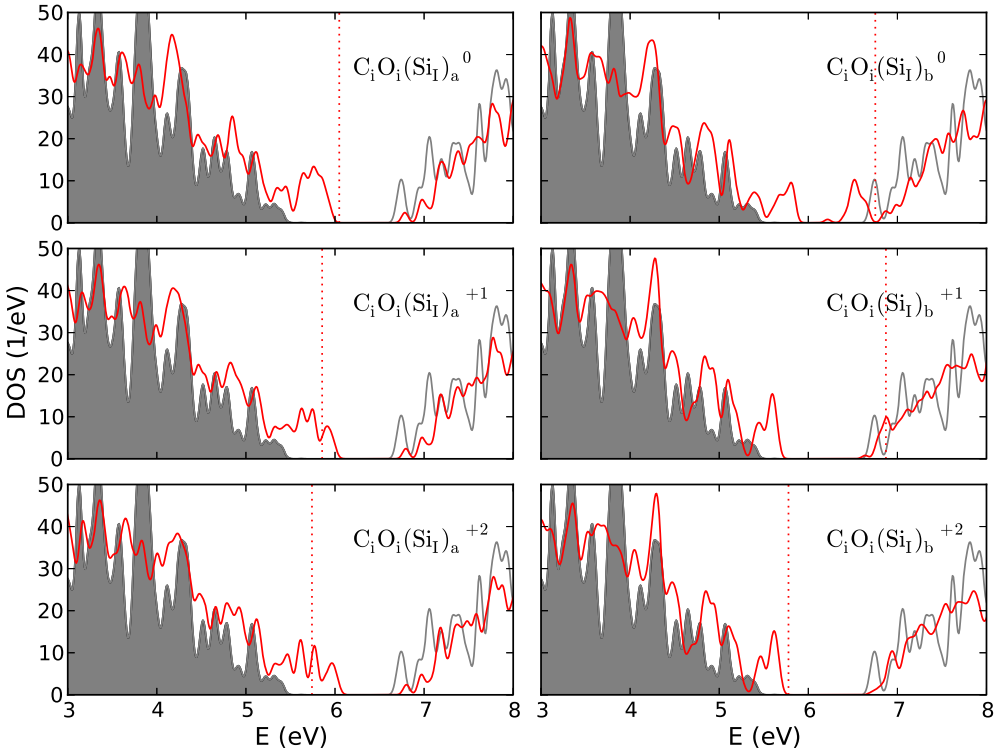

Figure 7 | Total DOSs of pristine Si (gray) and the $C_iO_i(Si_I)_a$ and $C_iO_i(Si_I)_b$ defects (red). The states left of the dotted line are occupied.

Figures 3(e), (f), and (g) present for different charge states the formation energy of the C_iC_s defect as a function of the Fermi energy. Note that for A-$C_iC_s^{+1}$, B-$C_iC_s^{-1}$, C-$C_iC_s^{0}$, $C_iC_s^{+1}$, and $C_iC_s^{-1}$ the energies from the spin polarized calculations are used. The results for the A- and B-type configurations are similar, because of the tiny total energy difference between them. An exception is that A-C_iC_s has a higher (+/0) transition level. For C-C_iC_s the +2 and −2 charge states are favorable below 0.06 eV and above 0.91 eV, respectively. The Fermi energy range in between is dominated by the 0 charge state, as spin polarization of the two unpaired electrons on the C atoms lowers the total energy significantly.

Defect clusters. Two configurations of $C_iO_i(Si_I)$, denoted as $C_iO_i(Si_I)_a$ and $C_iO_i(Si_I)_b$, see Figs. 1(c) and (d), are calculated. They are distinguished by the Si interstitial position relative to the C_iO_i pair and are similar to the C4(a) and C4(c) configurations reported by Backlund and Estreicher[25], respectively. In the figures the two Si atoms subject to a significant change in their position in the two configurations are marked in gray. The C and O interstitials form a ring with Si atoms. The four C-Si bond lengths are 1.84 Å, 1.85 Å, 1.89 Å, and 1.89 Å and the three O-Si bond lengths 1.77 Å, 1.79 Å, and 1.84 Å in $C_iO_i(Si_I)_a$, whereas in $C_iO_i(Si_I)_b$ the four C-Si bond lengths are 1.83 Å, 1.85 Å, 1.85 Å, and 1.91 Å and the three O-Si bond lengths 1.77 Å, 1.78 Å, and 1.84 Å. The total energy of $C_iO_i(Si_I)_a$ is always 0.28 eV lower than that of $C_iO_i(Si_I)_b$ for the 0, −1, and −2 charge states. However, $C_iO_i(Si_I)_a$ turns out to be 0.45 eV and 1.51 eV higher in energy than $C_iO_i(Si_I)_b$ for the +1 and +2 charge state, respectively. The formation energy as a function of the Fermi energy for the two $C_iO_i(Si_I)$ defect clusters is plotted in Figs. 3(c) and (d). $C_iO_i(Si_I)_a^{0}$ has a lower formation energy than $C_iO_i(Si_I)_b^{0}$, and a transition from the +2 into the 0 charge state is found for $C_iO_i(Si_I)_a$ as the Fermi energy increases. Transition levels between charge states are given in Table I. Still, $C_iO_i(Si_I)_b^{+2}$ dominates in the whole Fermi energy range.

Table IV | Binding energies (eV) and comparison to previous theoretical results

	This work	Literature
$C_i(Si_I)$	−2.34	−2.0[a]
C_iO_i	−1.60	−1.64[b]
A-C_iC_s	−1.07	−0.93[c], −1.34[d]
B-C_iC_s	−1.12	−0.95[c], −1.41[d]
C-C_iC_s	−1.68	−1.28[c], −1.76[d]
$C_iO_i(Si_I)_a$ (C_iO_i+Si_I)	−1.54	−1.50[b]
$C_iO_i(Si_I)_b$ (C_iO_i+Si_I)	−1.26	−1.11[b]
$C_iO_i(Si_I)_a$ (C_iSi_I+O_i)	−0.81	−1.57[b]
$C_iO_i(Si_I)_b$ (C_iSi_I+O_i)	−0.53	−1.18[b]

[a]Reference 27.
[b]Reference 25.
[c]Reference 31.
[d]Reference 49.

Total DOSs for the 0, +1, and +2 charge states of the two $C_iO_i(Si_I)$ configurations are shown in Fig. 7. In the structure of $C_iO_i(Si_I)_b^{0}$ the Si_I-C bond is oriented almost perpendicular to the C-O ring with a bond length of 1.91 Å, which is slightly larger than the calculated Si-C bond distance of 1.89 Å in face centered cubic SiC. The distances between Si_I and its Si neighbors are close to 2.50 Å (the shortest amounting to 2.44 Å), which is larger than the Si-Si bond length of 2.35 Å in the perfect lattice. This implies that Si_I interacts little with the surrounding Si atoms so that it can be considered to be isolated. Partial DOSs (not shown) demonstrate that the states between 6 eV and 6.8 eV in the case of $C_iO_i(Si_I)_b^{0}$ are defect states largely resulting from the isolated Si_I. We observe that the pseudo-gap between the valence band and the defect states increases in the +1 and +2 charge states. In the positively charged states the removed electrons stem mainly from Si_I. The Si_I-C bond length reduces from 1.91 Å in $C_iO_i(Si_I)_b^{0}$ to 1.87 Å in $C_iO_i(Si_I)_b^{+2}$, which indicates that the interaction between Si_I and C becomes stronger. The significant modifications of the electronic structure result in large energy gains for $C_iO_i(Si_I)_b^{+1}$ and $C_iO_i(Si_I)_b^{+2}$.

Comparing the atomic configuration of $C_iO_i(Si_I)_a^0$ to that of $C_iO_i(Si_I)_b^0$ shows that the isolated Si_I forces another Si off its lattice site, with a (101) symmetry plane. In the electronic structure the defect states shift to lower energy and merge to the valence band so that the donation of electrons is harder in $C_iO_i(Si_I)_a$. The stability of $C_iO_i(Si_I)_a$ and $C_iO_i(Si_I)_b$ in different charge states is determined by the competition between the energies associated with the defect states and the symmetry reduction. We observe that $C_iO_i(Si_I)_b$ is more stable than $C_iO_i(Si_I)_a$ in positively charged states, because electrons can be easier donated, which overcompensates the symmetry reduction. Nonetheless, $C_iO_i(Si_I)_a$ is more stable for other charge states due to its higher symmetry.

We find rather high values for the formation energies of the $C_i(Si_I)$, C_iO_i, C_iC_s, and $C_iO_i(Si_I)$ defects. For example, in the 0 charge states of $C_i(Si_I)$, C_iO_i, A-, B-, and C-C_iC_s, $C_iO_i(Si_I)_a$, and $C_iO_i(Si_I)_b$ they amount to 6.53 eV, 4.85 eV, 5.64 eV, 5.60 eV, 5.04 eV, 7.67 eV, and 7.95 eV, respectively. This is reasonable, because C_iO_i and C_iC_s pairs form under irradiation. Furthermore, when the irradiation dose is increased more Si self-interstitials are created and trapped by C_i and C_iO_i, to form $C_i(Si_I)$ and $C_iO_i(Si_I)$ clusters. This implies that the formation of $C_i(Si_I)$ and $C_iO_i(Si_I)$ requires more energy, consistent with our results. Binding energies for defect pairs and clusters are reported in Table IV, which includes also previous theoretical results for comparison. Note that the total energy of Si_I at the hexagonal site is taken to calculate the binding energies. While our results are largely in good agreement with other theoretical data, the significant difference to Ref. 25 concerning the $C_iO_i(Si_I)$ cluster relative to $C_i(Si_I)$ and O_i is due to the different structure of $C_i(Si_I)$ considered in this study.

In summary, HSE hybrid functional calculations have been employed to analyze the binding and formation energies of C-related defects in Si. The binding energy of the most stable structure of $C_i(Si_I)$ is calculated to be -2.34 eV, which is in line with the value of -2.0 eV in Ref. 27. A doubly charged state is favorable almost in the whole Fermi energy range. The $C_iO_i^{+1}$ defect is found to be favorable when spin polarization is taken into account, which lowers the total energy by prominent 0.25 eV. The unpaired electron is mainly localized on a C atom, leading to a local magnetic moment. The A- and B-type bistable C_iC_s structures are reproduced, where the HSE functional yields a significantly improved agreement with the experimental situation regarding the energetic order of the charge states, as compared to any previous theoretical prediction. In the case of the C-type C_iC_s configuration, two C atoms are not fully coordinated with localized dangling electrons. Spin polarization thus gives rise to a significant energy gain in the 0 charge state. For the $C_iO_i(Si_I)$ defect two possible structures have been addressed. In one case the Si_I turns out to become largely isolated from its atomic environment. As a consequence, the formation energy of the +2 charge state is strongly reduced and dramatic effects on the electronic structure are observed.

Methods

The Vienna Ab-initio Simulation Package[39] is employed with pseudopotentials generated by the projector augmented wave method[40]. For a $2 \times 2 \times 2$ supercell consisting of 64 Si atoms we use a $3 \times 3 \times 3$ k-mesh within the Monkhorst-Pack scheme[41] and a cutoff energy for the plane waves of 400 eV. All parameters have been converged carefully to guarantee an accuracy of 0.01 eV. The lattice constant of Si is optimized by the PBEsol[42] functional as it has been demonstrated to yield results close to those of very expensive hybrid functional HSE calculations[43,44]. For each charged defect, the pristine Si lattice constant is applied and the atomic positions are relaxed until the forces on all atoms have declined below 0.01 eV/Å. The optimized structures are then used for HSE calculations, which are capable of reproducing the experimental band gap of Si[35], with a screening parameter of 0.206 $Å^{-1}$, where the local contribution to the functional is treated on the PBE level[45]. The mixing parameter is set to 0.25. We apply the correction approach developed by Freysoldt *el al.*[46,47] for finite size supercell calculations to eliminate artificial interaction between charged defects due to the periodic boundary conditions.

The formation energy of the $C_i(Si_I)$, C_iO_i, C_iC_s, and $C_iO_i(Si_I)$ defects with respect to the Fermi energy for all possible charge states is given by[48]:

$$\Delta H(\mu_e,\mu_\alpha) = E_{D,q} - E_H + \sum_\alpha n_\alpha \mu_\alpha + q\mu_e \quad (1)$$

where $E_{D,q}$ is the total energy of the defective cell with charge q, E_H is the total energy of the perfect Si cell, n_α represents the numbers of atoms added to or removed from the defective cell, and μ_α corresponds to their chemical potentials. Moreover, μ_e is the Fermi energy and is measured from the valence band maximum, having values inside the band gap, $E_{VBM} \le \mu_e \le E_{VBM} + E_g$. The O and C chemical potentials are calculated using α-quartz SiO_2, as $(E(SiO_2) - 3\mu_{Si})/6$, and face centered cubic SiC, respectively.

A way to investigate the energetics of point defect association is the calculation of the binding energies of the clusters. For example, the binding energy of a C_i atom to a C_s atom to form a C_iC_s defect pair is given by

$$E_b(C_iC_sSi_{N-1}) = E(C_iC_sSi_{N-1}) - E(C_iSi_N) - E(C_sSi_{N-1}) + E(Si_N) \quad (2)$$

where $E(C_iC_sSi_{N-1})$ is the energy of an N site supercell (here $N = 64$) with $N-1$ Si atoms, one C_s atom and one C_i atom, $E(C_iSi_N)$ is the energy of a supercell containing one C_i atom and N Si atoms, $E(C_sSi_{N-1})$ is the energy of a supercell containing one C_s atom and $N-1$ Si atoms, and $E(Si_N)$ is the energy of an N atom Si supercell. With this definition a negative binding energy corresponds to a defect pair which is stable with respect to its constituent point defects.

1. Kolbersen, B. O. & Mühlbauer, A. Carbon in silicon: properties and impact on devices. *Solid State Electron.* **25**, 759–775 (1982).
2. Newman, R. C. Carbon in Crystalline Silicon MRS Proceedings. **59**, 403 (1985).
3. Newman, R. C. & Jones, R. "*Oxygen in Silicon*" in *Semiconductors and Semimetals,* Shimura F. (ed.), Vol. 42, 289 (Academic Press, Orlando, 1994).
4. Davies, G. & Newman, R. C. in *Handbook of Semiconductors*, Mahajan S. (ed.), Vol. 3, 1557–1635 (Elsevier, Amsterdam, 1994).
5. Scorupa, W. & Yankov, R. A. Carbon-mediated effects in silicon and in silicon-related materials. *Mater. Chem. Phys.* **44**, 101–143 (1996).
6. Londos, C. A. Aspects of the defect reactions related to carbon impurity in silicon. *Jpn. J. Appl. Phys.* **27**, 2089–2093 (1988).
7. Newman, R. C. & Bean, A. R. Irradiation damage in carbon-doped silicon irradiated at low temperatures by 2 MeV electrons. *Radiat. Eff.* **8**, 189–193 (1970).
8. Watkins, G. D. & Brower, K. L. EPR observation of the isolated interstitial carbon atom in silicon. *Phys. Rev. Lett.* **36**, 1329–1332 (1976).
9. Vook, F. L. & Stein, H. J. Infrared absorption bands in carbon-oxygen-doped silicon. *Appl. Phys. Lett.* **13**, 343–346 (1968).
10. Londos, C. A. Deep-level transient spectroscopy studies of the interstitial carbon defect in silicon. *Phys. Rev. B* **35**, 6295–6297 (1987).
11. Davies, G., Lightowlers, E. C., Newman, R. C. & Oates, A. S. A model for radiation damage effects in carbon-doped crystalline silicon. *Semicond. Sci. Technol.* **2**, 524–532 (1987).
12. Lavrov, E. V., Hoffmann, L. & Nielsen, B. Local vibrational modes of the metastable dicarbon center (C_s–C_i) in silicon. *Phys. Rev. B* **60**, 8081–8086 (1999).
13. Londos, C. A., Potsidi, M. S. & Stakakis, E. Carbon-related complexes in neutron-irradiated silicon. *Physica B* **340–342**, 551–555 (2003).
14. Liu, C.-L., Windl, W., Borucki, L., Lu, S. & Liu, X.-Y. Ab initio modeling and experimental study of C-B interactions in Si. *Appl. Phys. Lett.* **80**, 52–54 (2002).
15. Brotherton, S. D. & Bradley, P. Defect production and lifetime control in electron and γ-irradiated silicon. *J. Appl. Phys.* **53**, 5720–5732 (1982).
16. Trombetta, J. M. & Watkins, G. D. Identification of an interstitial carbon-interstitial oxygen complex in silicon. *Appl. Phys. Lett.* **51**, 1103–1105 (1987).
17. Jones, R. & Öberg, S. Oxygen frustration and the interstitial carbon-oxygen complex in Si. *Phys. Rev. Lett.* **68**, 86–89 (1991).
18. Coutinho, J. *et al.* Interstitial carbon-oxygen center and hydrogen related shallow thermal donors in Si. *Phys. Rev. B* **65**, 014109 (2001).
19. Leery, P., Jones, R., Öberg, S. & Torres, V. J. B. Dynamic properties of interstitial carbon and carbon-carbon pair defects in silicon. *Phys. Rev. B* **55**, 2188–2194 (1997).
20. Capaz, R. B., Dal Pino Jr, A. & Joannopoulos, J. D. Theory of carbon-carbon pairs in silicon. *Phys. Rev. B* **58**, 9845–9850 (1998).
21. Cloutier, S. G., Kossyrev, P. A. & Xu, J. Optical gain and stimulated emission in periodic nanopatterned crystalline silicon. *Nat. Mater.* **4**, 877–891 (2005).
22. Rotem, E., Shainline, J. M. & Xu, J. M. Enhanced photoluminescence from nanopatterned carbon-rich silicon grown by solid-phase epitaxy. *Appl. Phys. Lett.* **91**, 051127 (2007).
23. Berhanuddin, D. D., Lourenço, M. A., Gwilliam, R. M. & Homewood, K. P. Co-implantation of carbon and protons: an integrated silicon device technology compatible method to generate the lasing G-center. *Adv. Funct. Mater.* **22**, 2709–2712 (2012).
24. Murata, K., Yasutake, Y., Nittoh, K., Fukatsu, S. & Miki, K. High-density G-centers, light-emitting point defects in silicon crystal. *AIP Adv.* **1**, 032125 (2011).
25. Backlund, D. J. & Estreicher, S. K. C4 defect and its precursors in Si: first-principles theory. *Phys. Rev. B* **77**, 205205 (2008).
26. Backlund, D. J. & Estreicher, S. K. Theoretical study of the C_iO_i and $I_{Si}C_iO_i$ defects in Si. *Physica B* **401–402**, 163–166 (2007).

27. Mattoni, A., Bernantini, F. & Colombo, L. Self-interstitial trapping by carbon complexes in crystalline silicon. *Phys. Rev. B* **66**, 195214 (2002).
28. Londos, C. A., Potsidi, M. S., Antonaras, G. D. & Andrianakis, A. Isochronal annealing studies of carbon-related defects in irradiated Si. *Physica B* **376–377**, 165–168 (2006).
29. Londos, C. A., Fytros, L. G. & Georgiou, G. J. IR Studies of oxygen-vacnacy related defects in irradiated silicon. *Defect Diffus. Forum* **171–172**, 1–32 (1999).
30. Bean, A. R. & Newman, R. C. The solubility of carbon in pulled silicon crystals. *J. Phys. Chem. Solids* **32**, 1211–1219 (1971).
31. Zirkelbach, F. *et al*. Combined ab initio and classical potential simulation study on silicon carbide precipitation in silicon. *Phys. Rev. B* **84**, 064126 (2011).
32. Bar-Yam, Y. & Joannopoulos, J. D. Barrier to migration of the silicon self-interstitial. *Phys. Rev. Lett.* **52**, 1129–1132 (1984).
33. Leung, W.-K., Needs, R. J. & Rajagopal, G. Calculations of silicon self-interstitial defects. *Phys. Rev. Lett.* **83**, 2351–2354 (1999).
34. Voronkov, V. V. & Falster, R. Properties of vacancies and self-interstitials in silicon deduced from crystal growth, wafer processing, self-diffusion and metal diffusion. *Mater. Sci. Eng. B* **134**, 227–232 (2006).
35. Heyd, J., Peralta, J. E., Scuseria, G. E. & Martin, R. L. Energy band gaps and lattice parameters evaluated with the Heyd-Scuseria-Ernzerhof screened hybrid functional. *J. Chem. Phys.* **123**, 174101 (2005).
36. Mooney, P. M., Cheng, L. J., Süli, M., Gerson, J. D. & Corbett, J. W. Defect energy levels in boron-doped silicon irradiated with 1-MeV electrons. *Phys. Rev. B* **15**, 3836–3843 (1977).
37. Song, L. W., Zhan, X. D., Benson, B. W. & Watkins, G. D. Bistable interstitial-carbon–substitutional-carbon pair in silicon. *Phys. Rev. B* **42**, 5765–5783 (1990).
38. Burnard, M. J. & DeLeo, G. G. Interstitial carbon and the carbon-carbon pair in silicon: Semiempirical electronic-structure calculations. *Phys. Rev. B* **47**, 10217–10225 (1993).
39. Kresse, G. & Joubert, D. From ultrasoft pseudopotentials to the projector augmented-wave method. *Phys. Rev. B* **59**, 1758–1775 (1999).
40. Blöchl, P. E. Projector augmented-wave method. *Phys. Rev. B* **50**, 17953 (1994).
41. Monkhorst, H. J. & Pack, J. D. Special points for Brillouin-zone integrations. *Phys. Rev. B* **13**, 5188–5192 (1972).
42. Perdew, J. P. *et al*. Restoring the Density-gradient expansion for exchange in solids and surfaces. *Phys. Rev. Lett.* **100**, 136406 (2008).
43. Schimka, L., Harl, J. & Kresse, G. Improved hybrid functional for solids: the HSEsol functional. *J. Chem. Phys.* **134**, 024116 (2011).
44. Heyd, J., Scuseria, G. E. & Ernzerhof, M. Hybrid functionals based on a screened Coulomb potential. *J. Chem. Phys.* **118**, 8207–8215 (2003).
45. Perdew, J. P., Ernzerhof, M. & Burke, K. Rationale for mixing exact exchange with density functional approximations. *J. Chem. Phys.* **105**, 9982–9985 (1996).
46. Freysoldt, C., Neugebauer, J. & van de Walle, C. G. Fully ab initio finite-size corrections for charged-defect supercell calculations. *Phys. Rev. Lett.* **102**, 016402 (2009).
47. Freysoldt, C., Neugebauer, J. & van de Walle, C. G. Electrostatic interactions between charged defects in supercells. *Phys. Stat. Sol.* B **248**, 1067–1076 (2011).
48. Lany, S. & Zunger, A. Assessment of correction methods for the band-gap problem and for finite-size effects in supercell defect calculations: case studies for ZnO and GaAs. *Phys. Rev. B* **78**, 235104 (2008).
49. Sgourou, E. N. *et al*. Erratum "Impact of isovalent doping on the trapping of vacancy and interstitial related defects in Si" [J. Appl. Phys. 113, 113506 (2013)]. *J. Appl. Phys.* **113**, 239901 (2013).

Author contributions

H.W. performed the calculations and analysed the results together with A.C. and U.S. C.A.L. and E.N.S. contributed to the discussion. All authors have proofread the manuscript.

Additional information

Competing financial interests: The authors declare no competing financial interests.

How to cite this article: Wang, H., Chroneos, A., Londos, C.A., Sgourou, E.N. & Schwingenschlögl, U. Carbon related defects in irradiated silicon revisited. *Sci. Rep.* **4**, 4909; DOI:10.1038/srep04909 (2014).